

RESEARCH ARTICLE

The effect of local geometry and relative energy on grain boundary area changes during grain growth in SrTiO₃

Vivekanand Muralikrishnan  | Zipeng Xu | Gregory S. Rohrer  |
Amanda R. Krause 

Carnegie Mellon University, Pittsburgh,
Pennsylvania, USA

Correspondence

Amanda R. Krause, Carnegie Mellon
University, Pittsburgh PA 15213, USA.
Email: amandakr@andrew.cmu.edu

Funding information

National Science Foundation under
DMREF, Grant/Award Numbers: 2118945,
2246833; DOE Office of Science by
Argonne National Laboratory,
Grant/Award Number:
DE-AC02-06CH11357

Abstract

This study uses high-energy X-ray diffraction microscopy of SrTiO₃ to identify correlations between grain boundary (GB) area changes and the motion direction of neighboring GBs to investigate interfacial energy minimization mechanisms during grain growth. The local GB area changes were measured near triple lines (TLs) to isolate the effects of neighboring GBs. These area changes were then correlated to the migration direction and curvature of the neighboring GBs present at the TL, providing an alternative metric associated with lateral expansion for describing GB migration. Additionally, this study extracted GB dihedral angles, which reflect the relative GB energy, to test whether low energy GBs replace high energy GBs (i.e., GB replacement mechanism) and, thus, can be used to predict a GB's migration direction. The majority of GBs did not exhibit local area changes reflective of the GB replacement mechanism, and the dihedral angles were not reliable indicators of GB motion. However, the expansion and shrinkage of GBs moving away from their center of curvature was more often consistent with the grain boundary replacement mechanism. These results suggest that growth for certain GB configurations is governed by relative energy differences while others are governed by curvature.

KEYWORDS

microstructure, SrTiO₃, high energy X-ray diffraction microscopy, grain growth

1 | INTRODUCTION

The microstructure of a metal oxide affects its mechanical¹ and electrical^{2–4} properties. Hence, efficient microstructural design is essential for tailoring material performance. However, grain growth is still challenging to control or predict during processing. In the classical description of grain boundary (GB) migration, GBs move toward their

center of curvature, and their velocity is a product of their reduced mobility and curvature.^{5–8} However, recent experimental observations of GB migration using non-destructive 3D high energy X-ray diffraction microscopy (HEDM) in Ni,⁹ Fe,¹⁰ and SrTiO₃¹¹ polycrystals are not consistent with that description. Instead, they show (1) individual GB velocity is not linearly correlated with curvature, and (2) GBs do not always migrate toward their

This is an open access article under the terms of the [Creative Commons Attribution-NonCommercial](https://creativecommons.org/licenses/by-nc/4.0/) License, which permits use, distribution and reproduction in any medium, provided the original work is properly cited and is not used for commercial purposes.

© 2024 The Author(s). *Journal of the American Ceramic Society* published by Wiley Periodicals LLC on behalf of American Ceramic Society.

center of curvature. These observations suggest that the mechanism governing local GB migration is not well understood.

Most polycrystalline materials have anisotropic GB energy, such that neighboring GBs have competing driving forces to increase or decrease their areas, which complicates their motion. As discussed in the work by Niño and Johnson,¹² interfacial energy minimization during grain growth can occur by a combination of mechanisms, including:

1. Total GB area reduction,
2. Low energy GBs replace high energy GBs (GB energy replacement mechanism), and
3. GBs reorientation to a lower energy state.

By comparing simulations of grain growth with isotropic and anisotropic GB energy, Niño and Johnson report that area reduction is the dominant energy dissipation mechanism. However, indirect and direct observations find that, as the total GB area decreases, low energy GBs, on average, increase in relative area, and high energy GBs decrease in relative area in both experiments^{10,13–16} and simulations with anisotropic GB energy.^{17–22} Notably, HEDM observations in Ni by Xu et al.¹³ showed direct illustrations of low energy GBs expanding at the expense of their higher energy GB neighbors. Due to these observations, Xu et al.^{10,13} hypothesized that the GB replacement mechanism may be responsible for the anti-curvature GB motion observed in polycrystals. The purpose of this study is to determine if the expansion of relatively low energy GBs is associated with anti-curvature motion using HEDM measurements of grain growth in SrTiO₃.

To test this idea, this work first explores how the local area changes of a GB at a triple line (TL) correlate with the motion direction of its direct neighbors. It is expected that the growth of a grain can be described by the area reduction of the adjacent GBs. Similarly, GB should expand in area if it neighbors a shrinking grain. However, since a single GB touches many other grains, this study isolates the GB area changes around TLs. Then, the local GB area change is correlated to the dihedral angles at the TL, which provide a relative GB energy measurement, to test whether low energy GBs expand and high energy GBs shrink.

Only TLs with the topologies shown in Figure 1 are investigated for simplicity. The convex and concave topologies introduced in Figure 1 are classified based on how neighboring GBs in the TL are curved with respect to a common GB of interest. In the convex topology (represented by *VEX*), a GB of interest neighbors two GBs with mean curvatures that are convex with respect to their shared grain. Conversely, in a concave topology (represented by *CAV*), a GB of interest is neighboring two GBs

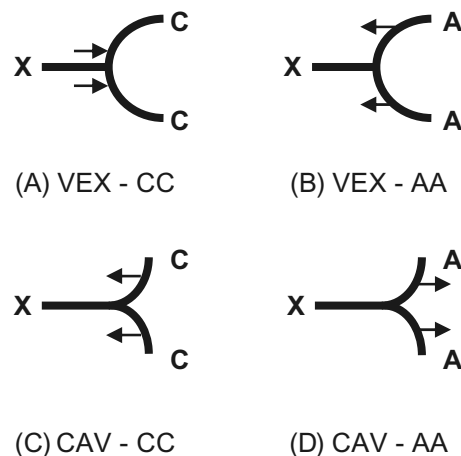


FIGURE 1 Schematic representation of the four-triple line (TL) configurations tested. The grain boundary (GB) of interest is indicated with an X. C and A represent GBs moving toward or away from their center of curvature, respectively. The motion direction of these GBs is indicated by the arrows. If X GB is bounded by a (A, B) convex "grain" (*VEX*), X is expected to expand and shrink if neighboring (A) CC and (B) AA GBs, respectively. Conversely, if X GB is bounded by a (C, D) concave "grain" (*CAV*), X is expected to shrink and expand if neighboring (C) CC and (d) AA GBs, respectively. The GB can be flat or curved in either direction.

with mean curvatures that are concave with respect to their shared grain. In both topologies, the GB of interest can be flat or curved in either direction. Additionally, the TLs are classified by the motion of the GBs neighboring the GB of interest. Those in which the two neighboring GBs move toward their center of curvature are labeled CC, whereas those in which the two neighboring GBs move away from their center of curvature (anti-curvature) are labeled AA. All other topologies or those in which the neighboring boundaries have mixed motion (one moves toward its center of curvature and the other against) are ignored for simplicity.

This analysis will compare the local area changes for the TL migration configurations. Then, the local GB area changes will be correlated to the initial GB dihedral angles. This analysis will potentially allow us to gain insights into the free energy minimization occurring during grain growth when GBs are bounded by GBs migrating toward their center of curvature and anti-curvature GBs.

2 | METHODS

2.1 | Material processing and HEDM data collection

The detailed processes for the sample preparation, data collection, reconstruction, and post-processing for SrTiO₃

HEDM data is described in an earlier publication.¹¹ Here, we will briefly describe the relevant sample details.

The bulk SrTiO₃ samples provided by Karlsruhe Institute of Technology were prepared by a solid-state synthesis route described in Reference [23]. To reach a reasonable grain size for characterization, the sintered sample was annealed at 1400°C for 10 h under flowing forming gas, after which the first HEDM map was collected. Then, the same sample was annealed in forming gas for an additional 70 h at 1400°C before the second HEDM measurement.

The HEDM maps were collected using the 1-ID beamline in the Argonne Photon Source at Argonne National Laboratory.²⁴ The diffraction data was reconstructed using the HEXOMAP software,²⁵ and the reconstructed data was imported into Dream3D (an open-source software)²⁶ for subsequent grain segmentation and post-processing steps as discussed below.

Grains were segmented by grouping contiguous voxels with a misorientation threshold of 1°. The voxel dimensions are 2 μm × 2 μm × 2 μm. Grains with fewer than 16 voxels were removed, and their voxels were distributed to neighboring grains in a dilation process. Similarly, grain dilation was performed to remove pores (unindexed regions) with fewer than four voxels.

2.2 | GB velocity, area, curvature, and dihedral angles calculations

To calculate GB velocity, grains were matched between the two measurements and the HEDM maps were aligned spatially. Grains were matched by finding pairs with similar misorientation (<1.5°) and centroid location (<20 μm). The microstructures are aligned by translating the second map by the average difference in centroid location between the matched grains. The GB velocity is determined by calculating the net volume of voxels flipped across the GB divided by the initial GB area.

GB area is determined by summing the area of all the voxel faces present at the GB of interest or within the volume of interest. GB curvatures and dihedral angles were calculated from the first collected HEDM map, before the observed growth. GB mean curvature is determined by calculating the integral mean curvature and dividing it by the initial GB area. Instead of smoothing or meshing the GB, the integral mean curvature (M_s) is computed for the voxelated structure, as described in Reference [27], using the Equation (1).

$$M_s = \frac{\pi}{4} (N_{outies} - N_{innies}), \quad (1)$$

where, N_{outies} is the total number of edges formed by convex voxel faces, and N_{innies} is the total number of edges formed by concave voxel faces at the GB of interest.

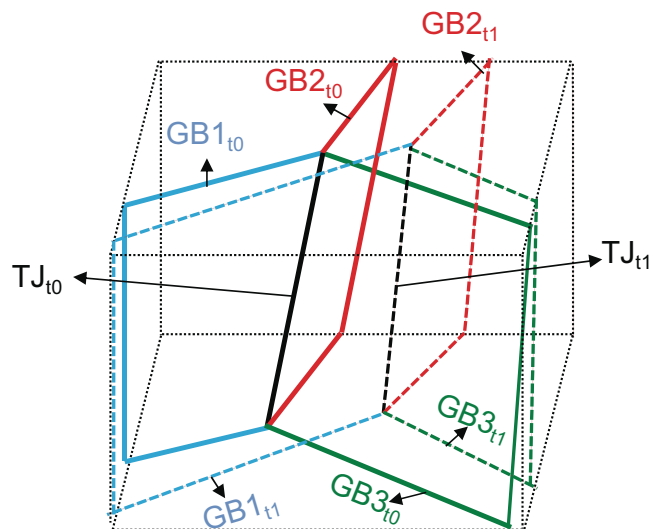


FIGURE 2 Schematic of constrained volume containing triple line (TL) found before (t_0 , grain boundary (GBs) bounded by solid lines) and after annealing (t_1 , GBs bounded by dashed lines) that is used for calculating local area changes. The local area change of GB1 (shaded in blue) is determined by the difference in GB area of the GB1_{t1} and GB1_{t0} within the constrained volume. Note that the end points of the TL are not included in the schematic for simplicity, but the entire TL is within the constrained volume for all calculations.

To calculate the GB dihedral angle, Matlab's MTEX package was used to extract the TL points' coordinates for each layer of the 3D microstructure map and the GB tangent vector near the TL points in each layer. The GB tangent vector was obtained after Laplacian smoothing the microstructure map of each layer for 25 iterations. The GB normal vector near the TL is obtained by calculating the cross product of the TL line vector with the GB tangent vector found. Then, the GB dihedral angles for the specific TL are calculated from the dot product of the GB normal vectors. The GB dihedral angle reported is the average value of those calculated at each layer containing the TL.

2.3 | Calculation for local GB area change

The local GB area change near a TL is calculated by the difference in GB area between the first and second HEDM maps within a constrained volume that contains the initial and final TL position (see Figure 2). Considering both positions in both timesteps, the minimum and maximum x , y , and z coordinates of the two TLs were identified. The bounds of the constrained volumes were set as the minimum and maximum coordinates, which were first rounded to the nearest integer and a single voxel was subtracted or added, respectively.

TABLE 1 The number of grain boundary (GBs) used in the dihedral angle and local area changes for the four different configurations in Figure 1. Note that the GB of interest may be *A* or *C* and the curvature is not constrained.

VEX or CAV	CC or AA	Number of GBs
VEX	CC	935
VEX	AA	623
CAV	CC	1003
CAV	AA	653

Abbreviations: AA, against their center of curvature; CC, move towards their center of curvature; CAV, concave topology; GB, grain boundary; VEX, convex topology.

2.4 | Classification and TL selection criteria

The GB's direction of motion is classified based on the sign of its velocity and the GB mean curvature product. If a GB moves toward its center of curvature (represented by *C*), the GB velocity and GB mean curvature have opposite signs with respect to the same reference grain such that their product is a negative value. Conversely, if a GB moves away from its center of curvature (anti-curvature GB motion, represented by *A*), the product of its velocity and curvature with respect to the reference grain is greater than or equal to zero. Note that a product of zero is considered anti-curvature because it indicates the motion of a flat boundary or a stationary curved boundary.

The GB dihedral angle and local area changes are compared for four different configurations shown in Figure 1: GBs bounded by concave GBs that either both moved toward their center of curvature (*CAV-CC*) or against their center of curvature (*CAV-AA*) and GBs bounded by convex GBs that either moved toward their center of curvature (*VEX-CC*) or against their center of curvature (*VEX-AA*). Table 1 reports the number of GBs used for the GB dihedral angle and local GB area change distributions for the different configurations tested.

3 | RESULTS AND DISCUSSION

Figure 3 compares the local GB area changes for the different configurations tested. On average, when the GBs are bounded by GBs migrating toward their center of curvature (*CC*, black curves in Figure 3), the *X* GBs with *VEX* topology increase in area, and the *X* GBs with *CAV* topology decrease in area. The GBs bounded by anti-curvature GBs (*AA*, red curves in Figure 3) show the opposite trends; on average, the *X* GBs with *VEX* topology decrease in area, and the *X* GBs with *CAV* topology increase in area. Note that the magnitude of area changes is greater for the *X*

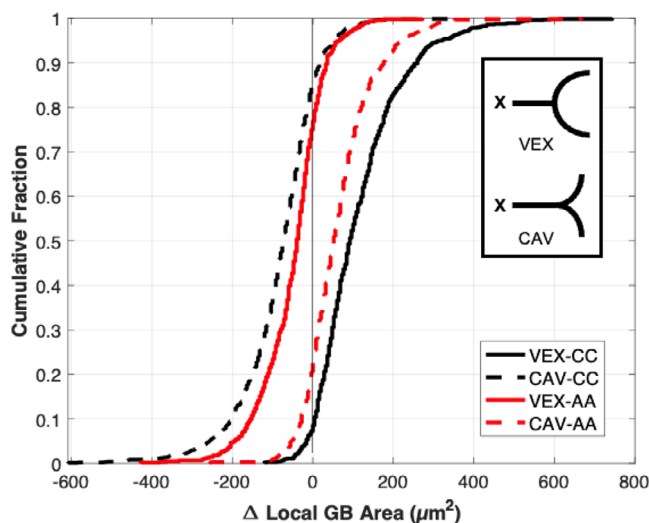


FIGURE 3 Cumulative distribution of the change in the local grain boundary (GB) area for the four-triple line (TL) configurations introduced in Figure 1.

GBs neighboring *CC* GBs than those neighboring *AA* GBs, irrespective of topology.

Figure 3 shows that, on an average, the local area change of a GB is related to the curvature and direction of motion of the neighboring GBs. For example, a GB is likely to expand if it neighbors a shrinking convex grain. Alternatively, the GB likely shrinks if its neighbor is a growing convex grain (anti-curvature motion). (Similar arguments can be made for GBs neighboring concave grains as shown in Figure 3.) This relationship holds for 83% of the GBs in this study, suggesting that the GB's lateral growth is important for elucidating the migration behavior. (Note that GB's area change is also dependent on the motion of adjacent TLs and its own migration, which may account for those GBs not conforming to this relationship.) If the GB replacement mechanism dominates, the inverse relationship would be true; the expansion of a low energy GB locally would cause the neighboring grain to shrink whether it be convex (following curvature) or concave (anti-curvature motion).

To test whether the observed correlation reflects the GB replacement mechanism, the dihedral angle distributions were used to classify GB energy. The GB dihedral angles are inversely related to the GB energy based on the Young's equation²⁸ as shown below in Equation (2).

$$\frac{\gamma_1}{\sin \theta_1} \equiv \frac{\gamma_2}{\sin \theta_2} \equiv \frac{\gamma_3}{\sin \theta_3}, \quad (2)$$

γ_1 , γ_2 , and γ_3 are the GB energy and θ_1 , θ_2 , and θ_3 are the corresponding GB dihedral angles of the three GBs meeting at the TL. This equation was derived based on the force equilibrium of the GBs at the TL and ignores any variation

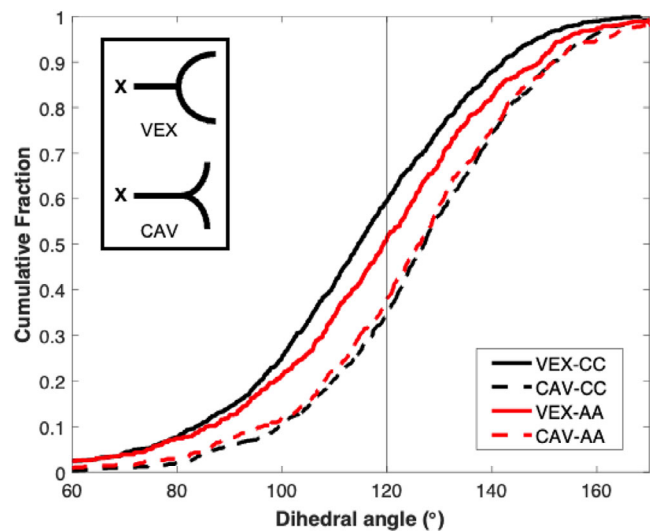


FIGURE 4 Cumulative distributions of dihedral angles for the four configurations introduced in Figure 1. These measurements were collected from the first 3D high energy X-ray diffraction microscopy (HEDM) map.

TABLE 2 The mean dihedral angle for grain boundaries (GBs) bounded by the different configurations.

CAV or VEX	CC or AA	Mean GB Dihedral Angle
VEX	CC	114°
VEX	AA	118°
CAV	CC	126°
CAV	AA	125°

Abbreviations: AA, move against their center of curvature; CC, move towards their center of curvature; CAV, concave topology; GB, grain boundary; VEX, convex topology.

in the GB energy with GB plane orientation. It is important to note that the dihedral angle provides the relative GB energy with respect to the neighbors present at that same TL. The absolute energy or the relative GB energy to the entire GB population is not known. However, since this study is concerned with the local migration behavior, dihedral angles are useful to determine whether a GB should want to expand or shrink given their neighborhood.

The dihedral angle distributions suggest that the relative GB energy and topology are correlated. Figure 4 and Table 2 compare the dihedral angle cumulative distributions and averages, respectively, for the different TL configurations. On average, GBs bounded by VEX GBs (solid lines in Figure 4) have a lower GB dihedral angle than GBs bounded by CAV GBs (dashed lines in Figure 4), irrespective of the different boundary migration conditions. Two sample Kolmogorov–Smirnov (KS) tests show that these distributions are statistically different (p -value $\ll 0.05$) when GBs have different GB topologies (Table 3).

TABLE 3 The p -values calculated from two sample Kolmogorov–Smirnov (KS) test comparing all possible combinations of the four configurations. The p -values less than 0.05 indicate the distributions are statistically different.

GB topology – TL migration configuration pairs for KS test		p -value
VEX-CC	VEX-AA	7×10^{-4}
CAV-CC	CAV-AA	0.5413
VEX-CC	CAV-CC	4×10^{-28}
VEX-CC	CAV-AA	2×10^{-18}
VEX-AA	CAV-CC	5×10^{-10}
VEX-AA	CAV-AA	7×10^{-6}

Abbreviations: AA, move against their center of curvature; CC, move towards their center of curvature; CAV, concave topology; GB, grain boundary; TL, triple line; VEX, convex topology.

These results support the conclusion that GBs bounded by VEX GBs, on average, have a higher relative GB energy than their neighbors, and GBs bounded by CAV GBs have lower relative GB than their neighbors.

In contrast to a previous study of grain boundaries in SrTiO_3 ,²⁹ the sample did not exhibit a strong anisotropy in the grain boundary plane or energy distributions. This is thought to reflect the difference in the partial pressure of oxygen during preparation (air in the previous work and forming gas here). Nevertheless, the dihedral angle distributions show systematic differences suggesting that the grain boundary energies cannot be considered isotropic, even if the variations are smaller than in previously studied materials.

According to the GB replacement mechanism hypothesis, the GBs bounded by CAV GBs are expected to increase in area because they are, in general, lower in energy relative to their neighbors. However, GBs bound by CAV-CC shrink on average. Similarly, the higher energy GBs (those bounded by VEX GBs) expand in area as their neighboring GBs move toward their center of curvature. These results indicate that factors other than the relative grain boundary energy, including geometrical constraints and curvature, influence grain boundary migration. Furthermore, these cases represent classes of triple lines where the local geometry is more influential than the relative energy.

In contrast, when bounded by anti-curvature boundaries (AA), lower energy GBs are more likely to expand, and high energy GBs are more likely to shrink. This can be seen by the GBs bounded by CAV, which are associated with lower energy, increasing in area. Similarly, GBs bounded by VEX GBs, which is the topology associated with higher energy, on average decrease in local area. Thus, for these classes of TLs, the relative energy is more important than local geometry in determining grain boundary migration.

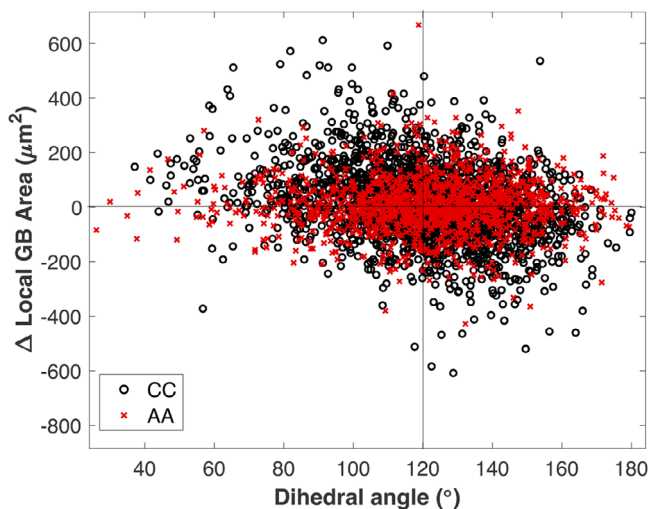


FIGURE 5 The change in local area for each grain boundary plotted with respect to its dihedral angle.

This trend for TLs with AA boundaries is not held when classifying GBs by their dihedral angles rather than topology; only half of GBs bounded with anti-curvature boundaries with dihedral angles greater than 120° and those with less than 120° increase and decrease, respectively, in local area. Figure 5 shows that the dihedral angle does not predict the expansion or shrinkage of a GB irrespective of the motion of its neighbors or topology. The GBs with the configuration associated with the lowest dihedral angles (*VEX-CC*, Figure 4) are more likely to expand rather than shrink when their neighbors move toward their center of curvature. Therefore, the dihedral angles, like curvature, cannot be used as an indicator of local GB area change or the motion direction of neighboring GBs.

This study finds that geometry (i.e., curvature) or relative energy governs motion for different classes of TLs. However, no clear indicator was found to identify which GBs will be dominated by relative energy instead of geometry. It is expected that GB replacement would dominate when the absolute difference in energy between neighboring GBs is high. Although providing energy information, the dihedral angles may not be indicative because they reflect the energy ratio rather than the absolute energy difference. For a given energy ratio, the absolute difference in energy can vary significantly depending on the minimum GB energy present. Given that SrTiO_3 is a polycrystalline ceramic primarily composed of general, high-angle GBs, the probability of a high energy GB neighboring two low energy GBs is low and, thus, unlikely to be reflected in the dihedral angle measurement. Therefore, it is possible that anti-curvature motion is associated with TLs that have the greatest absolute energy difference or the removal of the highest energy GBs, but not discernable from the measurements here.

4 | CONCLUSIONS

This work aimed to gain insights into the free energy minimization mechanism when GBs migrate toward and against their center of curvature in SrTiO_3 polycrystals as measured with HEDM. First, the local change in GB area was correlated to the motion direction of its neighboring GBs, irrespective of their curvature. This method provides an alternative metric to describe GB migration in terms of lateral motion rather than the typical velocity term associated with GBs moving perpendicular to their plane. To test whether GB motion direction is also correlated to the expansion of its low energy GBs neighbors (or the shrinkage of its high energy GBs neighbors), the local area change was compared to the GB's dihedral angle, which was used as an indicator of its relative GB energy. On average, anti-curvature motion is associated with the expansion of lower energy GBs and the shrinkage of higher energy GBs. However, most GBs investigated in this study do not show the relationship between the area change and the dihedral angle that is expected if GB replacement mechanisms were to dominate. Furthermore, individual dihedral angles, like curvatures, cannot be used as an indicator of local GB migration directions. Because the full GB energy function is not known, the analysis is limited to only consider the relative GB energy between neighbors and cannot isolate the behavior of truly low or high energy GBs, which may have an outsized role in the energy dissipation mechanism.


ACKNOWLEDGMENTS

This work was supported by the National Science Foundation under DMREF (grant no. 2118945 and 2246833). The Advanced Photon Source is a US Department of Energy (DOE) Office of Science User Facility operated for the DOE Office of Science by Argonne National Laboratory under contract no. DE-AC02-06CH11357.

ORCID

Vivekanand Muralikrishnan  <https://orcid.org/0000-0002-8086-9667>

Gregory S. Rohrer  <https://orcid.org/0000-0002-9671-3034>

Amanda R. Krause  <https://orcid.org/0000-0002-1503-8912>

REFERENCES

1. Bokov A, Zhang S, Feng L, Dillon SJ, Faller R, Castro RHR. Energetic design of grain boundary networks for toughening of nanocrystalline oxides. *J Eur Ceram Soc*. 2018;38(12):4260–67.
2. Tan Y, Zhang J, Wu Y, Wang C, Koval V, Shi B, et al. Unfolding grain size effects in barium titanate ferroelectric ceramics. *Sci Rep*. 2015;5(1):9953.

3. Luo J. Interfacial engineering of solid electrolytes. *J Materomics*. 2015;1(1):22–32.
4. Wang Z, Cao M, Yao Z, Li G, Song Z, Hu W, et al. Effects of Sr/Ti ratio on the microstructure and energy storage properties of nonstoichiometric SrTiO₃ ceramics. *Ceram Int*. 2014;40(1):929–33.
5. Burke JE, Turnbull D. Recrystallization and grain growth. *Prog Met Phys*. 1952;3:220–92.
6. Gottstein G, Shvindlerman LS. On the true dependence of grain boundary migration rate on driving force. *Scr Metall Mater*. 1992;27(11):1521–26.
7. Mullins WW. Two-dimensional motion of idealized grain boundaries. *J Appl Phys*. 1956;27(8):900–904.
8. Smith CS. Grain shapes and other metallurgical applications of topology. *Metallogr Microstruct Anal*. 2015;4(6):543–67.
9. Bhattacharya A, Shen YF, Hefferan CM, Li SF, Lind J, Suter RM, et al. Grain boundary velocity and curvature are not correlated in Ni polycrystals. *Science*. 2021;374(6564):189–93.
10. Xu Z, Shen YF, Naghibzadeh SK, Peng X, Muralikrishnan V, Maddali S, et al. Grain boundary migration in polycrystalline α -Fe. *Acta Mater*. 2024;264:119541.
11. Muralikrishnan V, Liu H, Yang L, Conry B, Marvel CJ, Harmer MP, et al. Observations of unexpected grain boundary migration in SrTiO₃. *Scr Mater*. 2023;222:115055.
12. Niño JD, Johnson OK. Influence of grain boundary energy anisotropy on the evolution of grain boundary network structure during 3D anisotropic grain growth. *Comput Mater Sci*. 2023;217:111879.
13. Xu Z, Hefferan CM, Li SF, Lind J, Suter RM, Abdeljawad F, et al. Energy dissipation by grain boundary replacement during grain growth. *Scr Mater*. 2023;230:115405.
14. Bojarski SA, Ma S, Lenthe W, Harmer MP, Rohrer GS. Changes in the grain boundary character and energy distributions resulting from a complexion transition in ca-doped yttria. *Metall Mater Trans A*. 2012;43(10):3532–38.
15. Muralikrishnan V, Langhout J, Delellis DP, Schepker K, Krause AR. Engineering grain boundary energy with thermal profiles to control grain growth in SrTiO₃. *J Am Ceram Soc*. 2024;107:7062–71.
16. Saylor DM, Morawiec A, Rohrer GS. The relative free energies of grain boundaries in magnesia as a function of five macroscopic parameters. *Acta Mater*. 2003;51(13):3675–86.
17. Kar D, Sintay SD, Rohrer GS, Rollett AD. Role of inclination dependent anisotropy on boundary populations during two-dimensional grain growth. *Mater Sci Forum*. 2012;715–716:697–702.
18. Holm E, Hassold GN, Miodownik MA. On misorientation distribution evolution during anisotropic grain growth. *Acta Mater*. 2001;49(15):2981–91.
19. Liu X, Wang J. Low-energy, mobile grain boundaries in magnesium. *Sci Rep*. 2016;6(1):21393.
20. Gruber J, George DC, Kuprat AP, Rohrer GS, Rollett AD. Effect of anisotropic grain boundary properties on grain boundary plane distributions during grain growth. *Scr Mater*. 2005;53(3):351–55.
21. Salama H, Kundin J, Shchyglo O, Mohles V, Marquardt K, Steinbach I. Role of inclination dependence of grain boundary energy on the microstructure evolution during grain growth. *Acta Mater*. 2020;188:641–51.
22. Naghibzadeh SK, Xu Z, Kinderlehrer D, Suter R, Dayal K, Rohrer GS. Impact of grain boundary energy anisotropy on grain growth. *Phys Rev Mater*. 2024;8(9):093403.
23. Bäurer M, Kungl H, Hoffmann MJ. Influence of Sr/Ti stoichiometry on the densification behavior of strontium titanate. *J Am Ceram Soc*. 2009;92(3):601–6.
24. Lienert U, Li SF, Hefferan CM, Lind J, Suter RM, Bernier JV, et al. High-energy diffraction microscopy at the advanced photon source. *JOM*. 2011;63(7):70–77.
25. Liu H, Suter R. HEXOMAP: High energy X-ray orientation mapping [Internet]. 2023 [cited 2023 Jun 24]. Available from: <https://github.com/HeLiuCMU/HEXOMAP>
26. Groeber MA, Jackson MA. DREAM.3D: a digital representation environment for the analysis of microstructure in 3D. *Integrating Mater Manuf Innov*. 2014;3(1):56–72.
27. Patterson B, DeHoff R, Sahi C, Sun J, Oddershede J, Bachmann F, et al. Integral mean curvature analysis of 3D grain growth: linearity of dV/dt and grain volume. *IOP Conf Ser Mater Sci Eng*. 2019;580(1):012020.
28. Smith C. Grains, phases, and interfaces—an interpretation of microstructure. *Trans AIME*. 1948;175:15–51.
29. Zhong X, Kelly MN, Miller HM, Dillon SJ, Rohrer GS. Grain boundary curvatures in polycrystalline SrTiO₃: dependence on grain size, topology, and crystallography. *J Am Ceram Soc*. 2019;102(11):7003–14.

How to cite this article: Muralikrishnan V, Xu Z, Rohrer GS, Krause AR. The effect of local geometry and relative energy on grain boundary area changes during grain growth in SrTiO₃. *J Am Ceram Soc*. 2025;108:e20319. <https://doi.org/10.1111/jace.20319>